Available online at www.sciencedirect.com
SCIENCE DIRECT®
Applied Surface Science 243 (2005) 166–177
applied surface science
www.elsevier.com/locate/apsusc

# Charging effects on electron-stimulated desorption of cations from gadolinia-doped ceria surfaces

Haiyan Chen[a], Yanfeng Chen[a], Alex Aleksandrov[a], Jian Dong[b], Meilin Liu[b], Thomas M. Orlando[a,*]

[a]*School of Chemistry and Biochemistry, Georgia Institute of Technology, 770 State Street, Atlanta, GA 30332, USA*
[b]*School of Materials Science and Engineering, Georgia Institute of Technology, Atlanta, GA 30332, USA*

Received in revised form 6 September 2004; accepted 12 September 2004

**Abstract**

Electron beam-induced charging and -stimulated desorption have been used to probe the electronic properties of gadolinia-doped ceria (GDC) surfaces. The main cationic desorption products resulting from electron bombardment are $H^+$, $H_3O^+$ and $O^+$. The dependence of the $H^+$ and $H_3O^+$ ion kinetic energies and yields on the surface potentials have been systematically investigated. Positive potentials increase the cation kinetic energies linearly while negative potentials reduce the cation yields dramatically. The charging of GDC by electron beam bombardment is dependent on the incident electron energy: negative at lower energy and positive at higher energy. Irradiation with 400 eV electrons can produce a positive surface potential of several volts while irradiation of the sample with 75 eV electrons can produce a negative sample potential of at least −6 V. The positive charge caused by high-energy electron irradiation can be neutralized by the negative charge generated by low-energy electrons and vice versa. The probable hole traps are sites close to $Gd^{3+}$, and the abundant presence of defects at oxygen vacancy-rich grain boundaries can serve as very effective electron traps.
© 2004 Elsevier B.V. All rights reserved.

*PACS:* 79.20.Kz; 81.05.Je

*Keywords:* Electron-stimulated desorption; Surface potentials; Gadolinia-doped ceria; Solid oxide fuel cells

## 1. Introduction

Solid oxide fuel cells (SOFCs) are highly efficient and environmentally benign chemical-to-electrical energy conversion devices with excellent fuel flexibility [1–6]. Largely due to their high operating temperatures (800–1000 °C), the cost of SOFC systems is still too high to be commercially viable. However, the interfacial polarization resistances of the current SOFCs increase rapidly as the operating temperature is reduced and severely limit fuel cell performance. In the search for SOFC materials suitable for low-temperature operation,

* Corresponding author. Tel.: +1 404 894 4012; fax: +1 404 894 7452.
*E-mail address:* thomas.orlando@chemistry.gatech.edu (T.M. Orlando).

0169-4332/$ – see front matter © 2004 Elsevier B.V. All rights reserved.
doi:10.1016/j.apsusc.2004.09.053

a fundamental understanding of the defect-mediated reactions at the surface and interface of electrolytes/electrodes is imperative. In particular, ceria-based solid electrolytes have attracted much attention [7] because of their high ionic conductivities at low temperatures. Among them, gadolinia-doped ceria ($Ce_{0.9}Gd_{0.1}O_{2-\delta}$, GDC) shows great promise for low-temperature SOFCs [8,9] and can thus serve as a model material for the exploration of surface properties relevant to electrochemical performance. Thus far, regarding surface reactions on GDC, only the oxygen surface exchange reaction has been investigated using isotope exchange depth profiling (IEDP) via secondary ion mass spectrometry (SIMS) [10–12]. With IEDP-SIMS, the activation energy for the oxygen surface exchange reaction was found to be 0.9eV for temperatures below 700°C and 3.3eV for temperatures above 700 °C. Similar energies were obtained for a single-crystal GDC ($Ce_{0.69}$ $Gd_{0.31}O_{1.845}$), i.e., 1eV for temperatures below 650°C and 2.41eV for temperatures above 650°C [11]. Apparently, the understanding of this surface oxygen exchange process at an electronic level has yet to be realized by other surface-specific analytical techniques.

Electron-stimulated desorption (ESD), or desorption induced by electronic transition (DIET), is an effective technique [13,14] that can provide valuable information on the structure of adsorbates and on the dynamics of charge transfer. Defects or local disorder on a surface, which may act as trapping sites of electronic excitations, can serve as preferential sites for desorption. Therefore, ESD can be a useful technique for exploring defects and their role in surface reactions critical for electrochemical performances of SOFCs.

For decades, ESD has contributed significantly to the study of the structure and the surface reactivity of non-stoichiometric and stoichiometric oxide surfaces. Since the electronic conductivity of most metal oxides is very low, very thin layers of metal oxides prepared by various deposition or growth techniques were used in many investigations in order to avoid the complications caused by surface charging. The structure and composition of these prepared oxides can vary and may be different from those used for industrial purposes. For the few studies done on bulk crystalline or amorphous dielectric oxide samples, unexplainable results were encountered even under standard conditions. For example, ESD of MgO(1 0 0) has been studied by Gotoh et al. [15] and $O^+$ desorption thresholds at 80 and 210 eV were found. These values are quite far from the Mg 2s excitation level at 50.8 eV. A similar study of MgO(1 0 0) surfaces obtained a 55 eV threshold after a +11 V correction for sample charge [16]. On the semiconductive $TiO_2$(1 1 0) surface, an onset at about 100 eV for $O^+$ ion desorption was observed after dosing CO. This threshold does not correspond to any core levels of either O or Ti [17]. In an ESD and photon-stimulated desorption study of yttria-stabilized $ZrO_2$(1 0 0), the sample was kept at 400–500 K to prevent charging [18], and thresholds at the Zr 4p and O 2s levels were observed.

In this paper, we present a study of electron-induced surface charging effects on the electron-stimulated desorption of cations from the surfaces of GDC, a dielectric metal oxide. For this defective metal oxide, surface charging depends strongly on incident electron energy and other parameters such as current density, pulse length and irradiation time. The results illustrate the influence of charging on the kinetic energies and yields of ejected ions. Collectively, the results reveal details regarding electronic properties of the surface.

## 2. Experimental

### 2.1. Sample preparation and characterization

The $Ce_{0.9}Gd_{0.1}O_{2-\delta}$ (GDC) samples were prepared using a glycine–nitrate process as described elsewhere [9]. Briefly, a flammable solution containing metal (Ce, Gd) nitrate and glycine was combusted in a glass beaker on a hot plate, producing a pale-yellow ash, which was then calcined in air at 600 °C for 2 h to form the fluorite structure. The resulting GDC powder was then ball-milled and cold-pressed into cylindrical pellets under 250 MPa. The green pellets were subsequently fired at 1250–1450 °C for 5 h with a heating and cooling rate of 5 °C/min in air to achieve greater than 95% relative density. The crystal structure of the GDC samples was studied using X-ray diffraction (XRD, PW-1800 system, with Cu Kα radiation operated at 40 kV and 30 mA), and the morphologies of the sintered

samples were revealed using a scanning electron microscope (SEM, Hitachi S-800).

### 2.2. Electron-stimulated desorption (ESD)

The ESD measurements were carried out in an ultra-high vacuum chamber (base pressure $2 \times 10^{-10}$ Torr) equipped with a rotatable helium-cooled sample holder, computer-controlled resistive tungsten sample heater or button heater, quadrupole mass spectrometer (QMS), time-of-flight (TOF) mass spectrometer, pulsed low-energy electron gun and a calibrated dosing system. Details of the system have been discussed elsewhere [19].

The dimensions of the GDC sample used for the ESD experiments were 10 mm × 6 mm and the thickness was ~1 mm. The GDC sample was mounted to a conductive molybdenum plate which was used to heat the sample and to apply the bias. The sample was annealed to 400 °C to clean the surface and the ESD of $H_3O^+$ and $O^+$ was measured at room temperature (300 K) while the proton ESD was studied at 230 K. Irradiation of the sample (grounded or with an externally applied potential) was performed by the pulsed electron beam operated at 1000 Hz. The electron energy, flux and pulse length were varied over a wide range, depending on the purposes of the experiment. Typical operating conditions were $10^{13}$ electrons/($cm^2$ s) during a given pulse or time-averaged currents of 20 pA to a few nano-amperes. Variation of the electron flux was performed exclusively by changing the gun emission current. Since we utilized a pulsed electron beam, the ESD of ions was measured by either a TOF or (QMS), both with better than unit mass resolution. When using the TOF, emitted ions were usually collected by applying a −100 V pulsed extraction potential to the front lens assembly. The −100 V potential was high enough to ensure a large solid angle of collection and to rule out any discrimination against off-normal trajectories or ion angular distribution effects. The extraction pulse was applied just after the end of the electron pulse to avoid the influence of the potential field on the incident electron energy. All ions were detected using pulse counting and a transient digitizer.

No extraction pulse was used to measure accurate kinetic energy distributions of emitted ions. Since detection sensitivity is reduced under field-free conditions, only the velocity distribution of the departing protons and hydroxonium ($H_3O^+$) was measured. When using the QMS as a mass analyzer, the ions were detected with its ionizer turned off. Calculations of ion velocities (and thus kinetic energy) from the TOF and QMS were based on known path lengths from the sample to the detector and measured flight times.

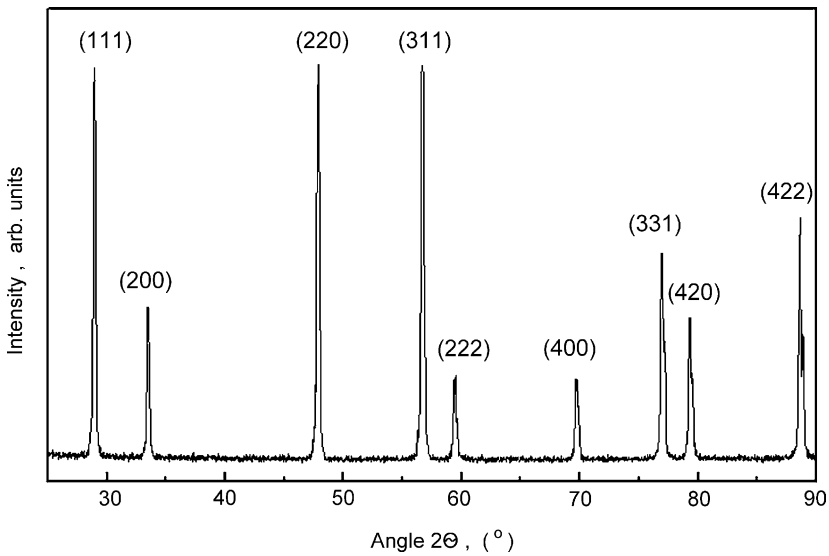


Fig. 1. X-ray diffraction pattern of a sintered $Ce_{0.9}Gd_{0.1}O_{2-\delta}$ (GDC) pellet which indicates the fluorite structure.

## 3. Results and discussion

### 3.1. Sample characterization

Fig. 1 shows a typical XRD pattern of a GDC sample, indicating that it has a single-phase fluorite structure, the same as that of $CeO_2$. Shown in Fig. 2 is the SEM image of the surface morphology of an as-sintered GDC sample. The grain size varies from 1 to 5 μm, and the sample has a significant number of grain boundaries and triple junctions. According to the electron energy loss spectroscopy (EELS) profile across the grain boundary [20], there is an excess of oxygen vacancies and gadolinium cations in the grain boundary core. The width of the grain boundary core is about a few nanometers while the width of the depletion layer can be larger than 15 nm. Assuming an average grain size of ∼2 μm with its surface dominated by structural defects that can trap free charges at a density of ∼10 traps/nm$^2$, the volumetric trap density is estimated to be $\sim 10^{18}$–$10^{19}$ traps/cm$^3$. A scanning tunneling microscopy (STM) study revealed that the dominant defects on the surface of non-stoichiometric $CeO_2$(1 1 1) are triangular with three oxygen vacancies at room temperature and linear at elevated temperatures [21]. The defect structure of the GDC grain should be close to that of the non-stoichiometric $CeO_2$, but the defect structure of the grain boundary can be very complicated.

### 3.2. ESD of cations

Electron irradiation of polycrystalline GDC causes emission of atomic and molecular ions. The dominant

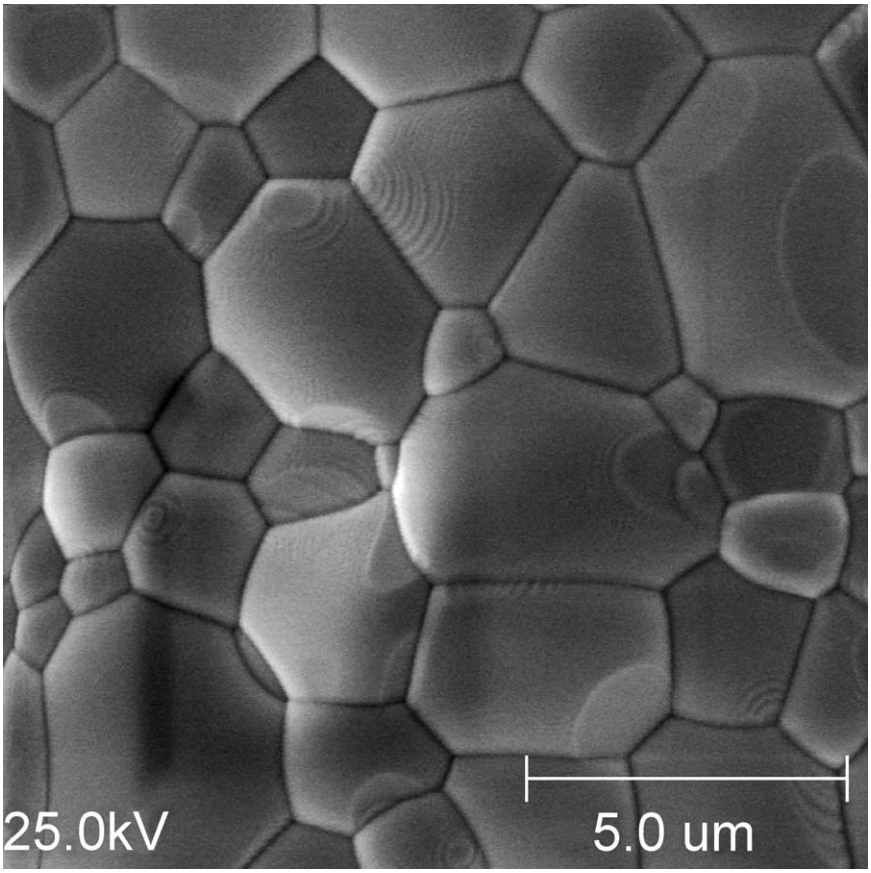


Fig. 2. SEM image of the morphology of a sintered $Ce_{0.9}Gd_{0.1}O_{2-\delta}$ (GDC) pellet which shows that the sample has a significant number of defective grain boundaries and triple junctions on its surface.

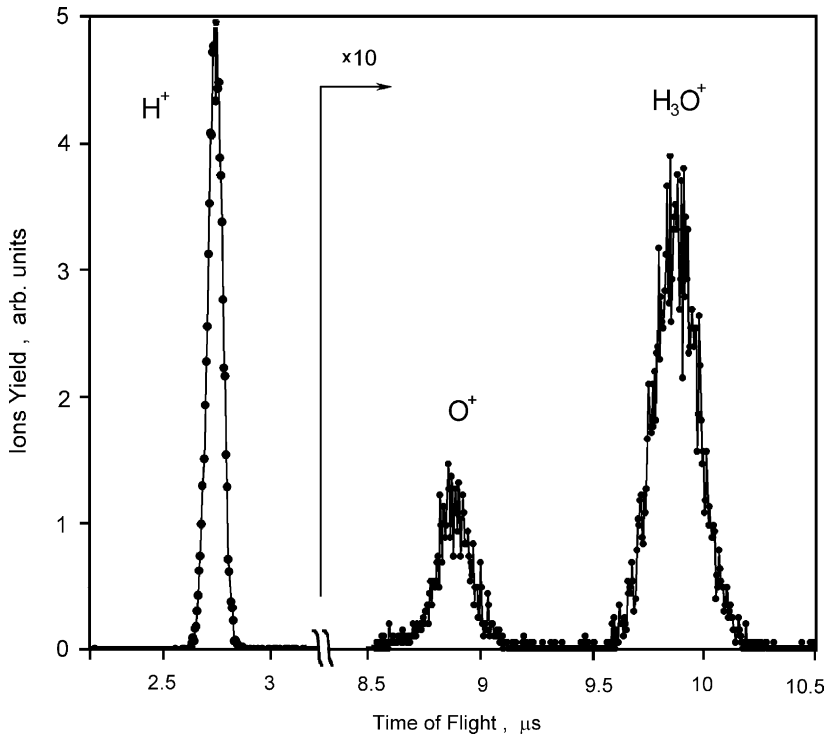


Fig. 3. Typical TOF-ESD spectrum of ions emitted from the GDC surface under the irradiation of 400 eV electrons. Note the yield of $H^+$ is considerably higher than the yield of all other cation products. The mass assignments were also confirmed with a quadrupole mass spectrometer.

positively charged ions emitted from this annealed substrate are protons. Compared to proton emission, the emission of other ions, mainly $H_3O^+$ and $O^+$, occurs with 1–2 orders of magnitude less efficiency (Fig. 3). The experimental primary threshold energy for proton ESD from GDC is 22 eV, and is associated with an initial ionization of the O 2s level that Auger decays. The proton desorption involves the production of two-hole states localized on hydroxyl groups which Coulomb explode directly at the surface. The $O^+$ threshold energy is also 22 eV, corresponding to direct ionization of O 2s, Ce 5p or Gd 5p levels followed by an intra-/inter-atomic Auger cascade [22]. The threshold energy appears to be lower than 22 eV for the molecular ion $H_3O^+$. The $H_3O^+$ ESD likely involves the chemisorption of water dimers that bridge surface anion vacancies. We suggest that the dimer may be polarized by the crystal field with the negative side of the $[OH^- \cdots H_3O^+]$ dipole oriented toward the oxygen vacancy [23]. At electron energies below the O 2s threshold, ionization of the lattice site in the vicinity of an adsorption complex can cause emission of the $H_3O^+$ fragment. At higher energies, ESD of $H_3O^+$ most likely proceeds by the two-hole one-electron states of water [24].

### 3.3. Effect of positive potentials

Although the masses of the ionic ESD products differ, they all have non-thermal kinetic energy distributions. The kinetic energy of an emitted ion often yields direct information concerning its formation mechanism. However, the energy of an ion at the point of its detection can differ from the energy at the point of its emission. Both the extraction potential applied to the detecting device and the surface potential induced by incident electrons can be integrated into the experimentally measured kinetic energy. The influence of extraction potential on ion energy can be evaluated experimentally. However, it is more complicated to assess the influence of surface potentials originating from the differentials between

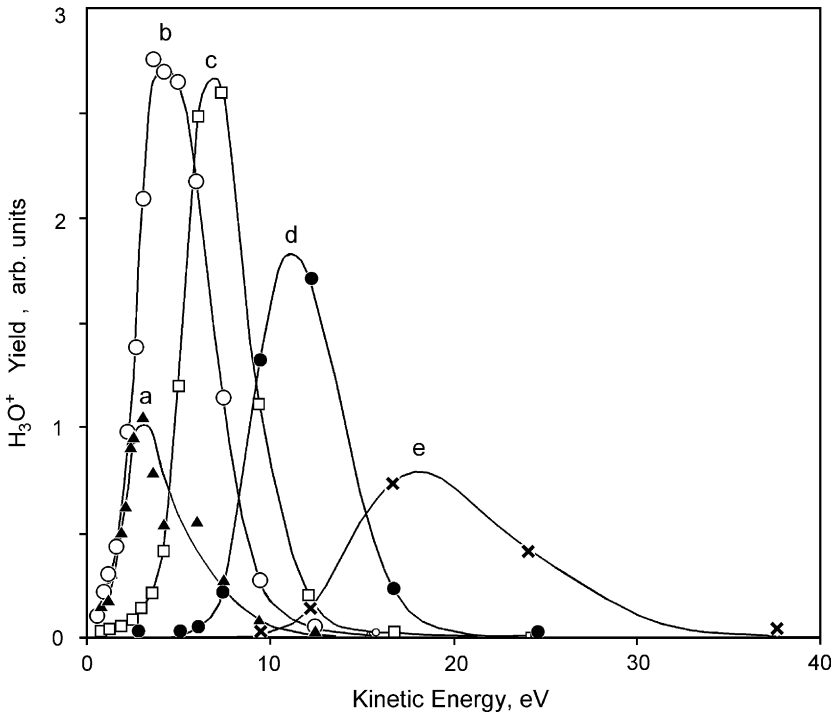


Fig. 4. Kinetic energy distributions of $H_3O^+$ as a function of different applied external positive potentials. The incident electron energy was 400 eV and the electron beam pulse length was 10 μs. Applied external potentials were: (a) 0 V; (b) 2 V; (c) 4 V; (d) 8 V; (e) 16 V.

the fluxes of primary electrons, low-energy secondary electron emission, backscattered electrons and electrons conducted through the sample to/from ground.

To investigate the influence of electron-induced surface potentials on the ESD of ions, constant external (positive and negative) potentials were applied to the sample during irradiation while TOF-ESD spectra were recorded. The kinetic energy distributions of $H_3O^+$ as a function of applied positive potentials are presented in Fig. 4. The sample potential dramatically changes the peak positions, and the peak kinetic energy depends linearly on the potential. The half-widths of the peaks increased with sample potential, probably indicating elevated heterogeneous charging caused by the larger sample bias. When a positive sample potential was applied to the back plate, transport of holes to the surface can be enhanced. The inhomogeneous positive charge built up at different sites can then reach a higher level at a larger bias, and can cause broadening of the kinetic energy distributions of desorbing cations. The ion yields approximately doubled when the sample potential was increased from 0 to 2 V. Since hole localization is always involved in the emission of cations, this yield increase may suggest that the holes can be trapped in shallow potential wells of surface states. The positive external electric field can suppress the diffusion of holes into the bulk and therefore can increase the number of holes on the surface that can induce ion emission. Similar data regarding the application of a positive potential was observed for $H^+$ ESD.

Surface potentials induced by the incident electron beam are expected to influence the kinetic energies of the emitted ions. For GDC, the average surface potential resulting from pulsed irradiation of 400 eV electrons was found to be positive. The influence of the electron flux on the $H_3O^+$ kinetic energy distributions and ESD yields is presented in Fig. 5. The higher the electron flux, the higher the ion kinetic energy, and the higher the positive charge accumulation. When the electron flux was increased from

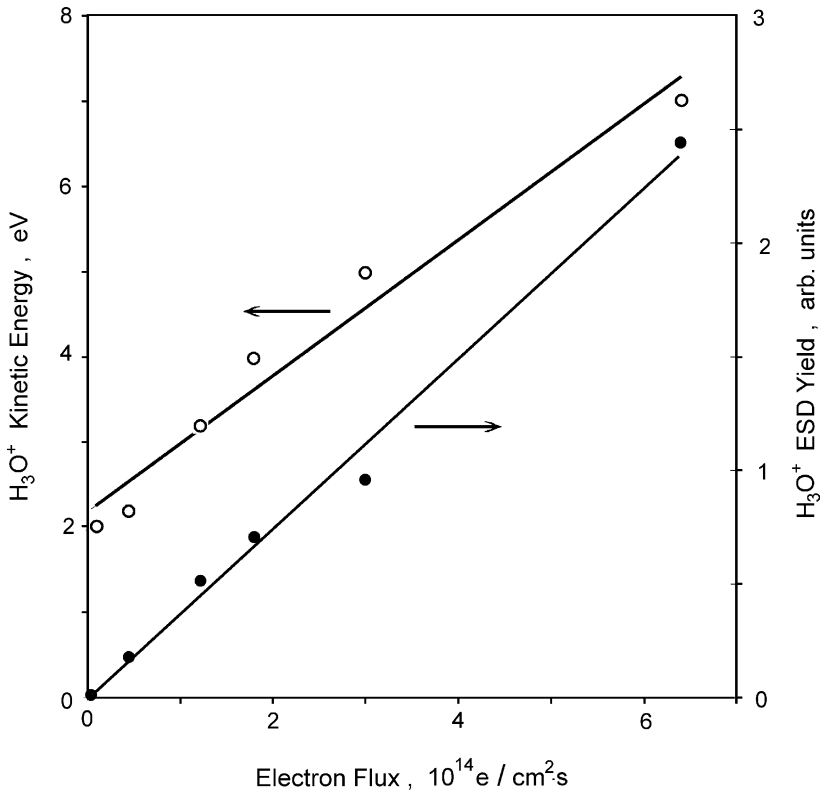


Fig. 5. Influence of electron flux on the peak kinetic energy and ESD yield of $H_3O^+$. The incident electron energy was 400 eV and the electron beam pulse length was 10 μs.

$4 \times 10^{12}$ to $3 \times 10^{14}$ electrons/($cm^2$ s), the change of surface potential caused by electron bombardment was estimated to be ~+3 V. The linear dependence of $H_3O^+$ yields on electron flux indicates that $H_3O^+$ is formed by a single direct impact ionization process. The positive charging of the GDC suggested the trapping of holes. In principle, holes should be trapped at sites with negative effective charge. For GDC, the most probable hole traps would be close to $Gd^{3+}$, and the most probable form would be $O^-$. Another possible form may be $O_2^-$ at the anion site. Electron spin resonance (ESR) experiments on the hole trapping in $Al_2O_3$ and $ZrO_2$ showed that the hole-induced charge has a diamagnetic character. The charge was therefore believed to be related to metal ions or to protons resulting from the interaction of the hole with metal–hydrogen bonds [25,26]. Metal ions or protons may be other forms of hole trapping in GDC.

### 3.4. Effect of negative potentials

Application of negative potentials to the sample under irradiation of 400 eV electrons caused significant decreases in the ion yields, as demonstrated in Fig. 6. The $H_3O^+$ yields decrease exponentially with the sample potential, indicating recapture or neutralization by the surface. Using no extraction field, with a −6 V applied sample potential, 99% of the ions were recaptured. Similar data were also obtained for $H^+$. Application of negative potentials also caused the flight time of ions to increase, as is shown for $H^+$ in Fig. 7. The apparent peak kinetic energy of $H^+$, expressed as the inverse of the square of the peak flight time, depends linearly on the applied negative potential. With −100 V extraction potential applied to the TOF entrance grid, 99% of the ions were recaptured when the applied negative potential was −30 V.

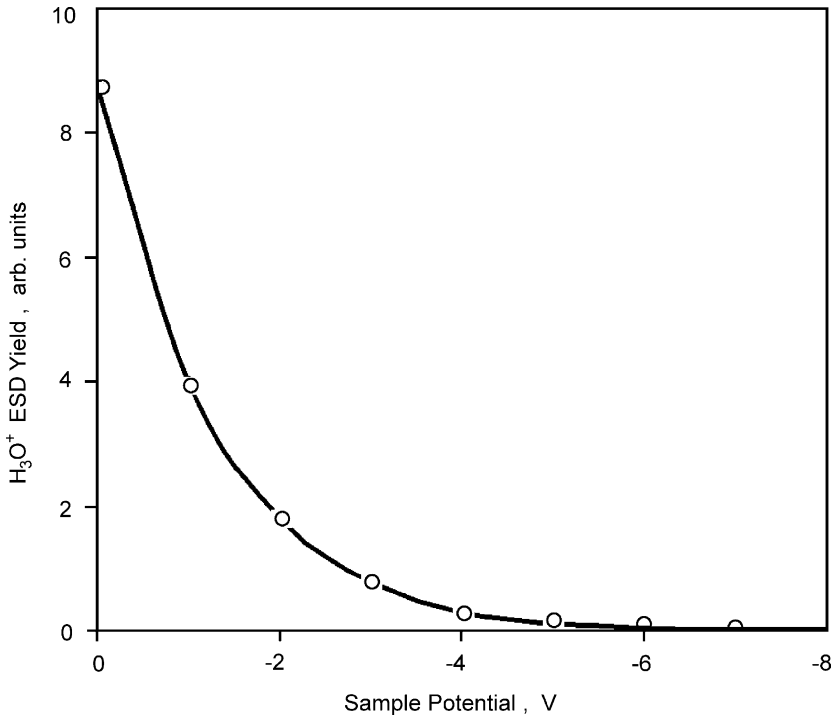


Fig. 6. Influence of negative sample potential on the $H_3O^+$ ion yield. The incident electron energy was 400 eV and the electron beam pulse length was 10 μs. Note 99% of the $H_3O^+$ yield is suppressed with the application of ∼−6 V external potential.

Electrons with an incident energy of 75 eV were chosen to further investigate the negative surface potential caused by electron bombardment. Electrons of lower energies are reflected significantly by the built-up negative charge and are retarded in the potential field of the surface. Irradiation with electrons of higher energies is less efficient in charging the sample negatively because of increased emission of secondary electrons. The sample was pretreated with 200 eV electron irradiation to ensure that the surface is not initially negatively charged. After this pretreatment, the sample was subjected to irradiation of 75 eV electrons, and the TOF spectra were obtained periodically. In order to enhance the detection sensitivity, a −100 V extraction potential was applied to the entrance grid of the TOF mass spectrometer immediately after the 75 eV electron beam pulse. The variation of the normalized ion yields versus total number of 75 eV electrons incident on the surface is presented in Fig. 8. This shows three distinct features of the ion yield dependence on the total number of electrons deposited. The first is a relatively slow monotonic decrease of the ion yield with increasing electron dose until the total dose of $1.2'10^{15}$ electrons/$cm^2$ is reached. During this process, the total drop of the ion yields is less than 50% for both $H^+$ and $H_3O^+$. The second feature is a drastic drop of ion yields when the electron dose was increased from $1.2 \times 10^{15}$ to $1.36 \times 10^{15}$ electrons/$cm^2$. The last feature shows that 99.9% of ion emission is suppressed after the total dose of electrons is greater than $1.36 \times 10^{15}$ electrons/$cm^2$.

The first feature can be explained by a charge neutralization process. Before the 75 eV electrons were deposited, the surface is positively charged due to the pretreatment with 200 eV electrons. With the deposition of 75 eV electrons, the peak flight time of the ions was increased (or the kinetic energy was decreased), indicating a decreased surface potential and therefore a decrease in the number of positive charges on the surface. If the surface is not positively charged during this stage, and if the negative charge build-up is a linear process, the ion yields should drop exponentially with the electron dose, which was not

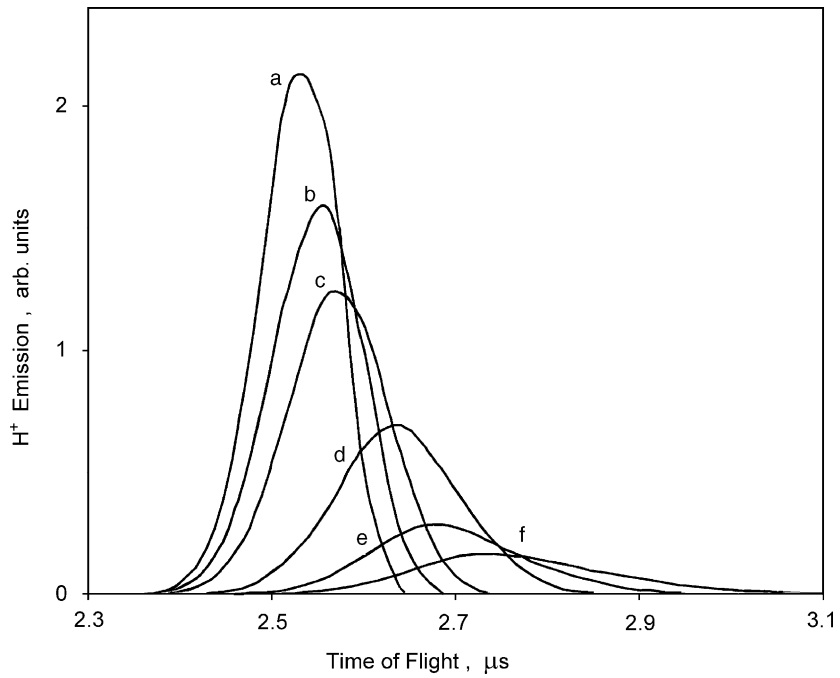


Fig. 7. Influence of an externally applied negative potential on the TOF spectra of $H^+$. The incident electron energy was 400 eV, the electron beam pulse length was 300 ns and the extraction field was −100 V. The external potentials were: (a) 0 V; (b) −2 V; (c) −4 V; (d) −10 V; (e) −15 V; (f) −20 V.

observed experimentally. For longer pretreatment time, higher doses of 75 eV electrons are required to cause ∼50% drop in the ESD ion yields, as is consistent with neutralization of an initial positive charge. The different influence of charge build-up on the ion yields of $H^+$ and $H_3O^+$ might be associated with the different mechanisms of ion formation at different emission sites.

The sudden drop off of Fig. 8 is caused mainly by the recapture of the emitted ions by a 75 eV electron beam-induced negative surface potential field. The ion yield does not drop exponentially with the electron dose, possibly because of a nonlinear charge build-up process as well as the backscattering of 75 eV electrons by the negative potential. A 99% drop in ion yields means that 75 eV electrons can charge the surface to such a level that the ion emission is actually quenched. The ion emission quenching is sustained as long as the 75 eV electrons are deposited to the GDC surface. After the ion emission was quenched, the intensity and peak flight time of the ESD ion signal could be restored completely by bombarding the GDC surface with 200 eV electrons. This observation indicates that the type and amount of charge on GDC surface could be manipulated by bombardment with electrons with different energies.

When the incident electron energy was 400 eV and no extracting potential was used, application of a ∼−6 V negative potential to GDC sample completely suppressed the ESD of $H_3O^+$ (Fig. 6). Since the ion emission was quenched by the irradiation with 75 eV electrons, it means that the surface was charged to at least −6 V during the pulse of the electrons. Simple calculations show that the number of electrons reaching the surface during the period of a single pulse is high enough to cause local surface charging up to several volts in the area of the electron beam. Average spreading of the primary electrons inside a crystal during the inelastic scattering and thermalization to the Debye temperature (10–30 meV) occurs within $\sim 10^{-12}$ s and does not exceed 50–100 nm. The migration of the thermalized free electrons has a diffusive character due to elastic scattering by optical phonons. Assuming that the mean free path of the

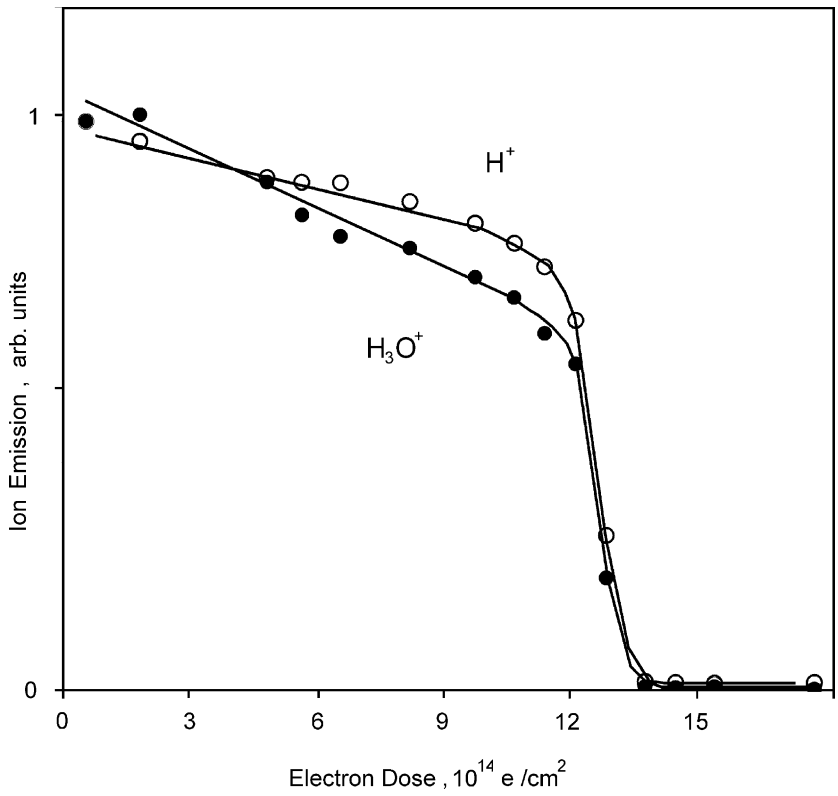


Fig. 8. The dependence of normalized ion yield on electron dose. The incident electron energy was 75 eV, the electron beam pulse length was 300 ns and the extraction field was −100 V. The significant decrease of ion yield implies the trapping of electrons by GDC.

electron is close to the one observed for alkali halide crystals, i.e. about 1–3 nm [27], the average mean-square shift of the scattered electrons between pulses ($10^{-3}$ s) is evaluated to be $10^{-4}$–$10^{-3}$ m, not far from the thickness of the sample. The potential field generated by the electron pulse that followed can repel the free electrons to ground. However, due to the presence of abundant different types of structural defects in GDC, thermalized electrons could be in traps with different depths. Electrons trapped by a deep potential well cannot be driven to ground and can thus form a long-lived negative charge inside or on the sample.

### 3.5. Role of defects

Negative surface charging of various materials, such as ice [28], plastics bombarded with low-energy electrons (0.1–28 eV) [29], single-crystal oxides bombarded by 30 keV electron beam [30] and thin layers of oxides on dielectric substrates [31] have been observed. When there are no surface defects, secondary electrons are able to be emitted from the bulk of the sample to the vacuum, reducing the trapping yield even to zero. When a defective layer exists at the surface of the sample, it acts as a barrier against the outgoing secondary electrons. Some of the secondary electrons are trapped beneath the surface, at the interface between the defective layer and the bulk. The probability of trapping free electrons can be very high for GDC, a low conductivity oxide with a highly defective surface area. Molecular dynamics simulation of gadolinia-doped ceria predicted the segregation of gadolinium and the association of oxygen vacancies with gadolinium [32]. This segregation effect at grain boundaries in $Gd_{0.2}Ce_{0.8}O_{2-x}$ was indeed observed and was characterized by a combination of Z-contrast imaging and electron energy loss spectroscopy (EELS) [20]. The composition profile obtained by EELS spectra showed that there is an excess of Gd and

oxygen vacancies in the grain boundary core. The gadolinium segregated to the grain boundary partially compensates for the oxygen vacancies, but the level for segregation is insufficient to charge balance the vacancies. Because the oxygen vacancies have positive effective charges, vacancy-rich grain boundaries can serve as very efficient electron traps and charge the sample negatively. The sites close to $Gd^{3+}$, which are also located at grain boundaries, are most probable traps for holes. Therefore we believe the charging effect that we observed occurs primarily at the grain boundaries. Since grain boundaries can trap charge more efficiently, the conduction of electrons or holes by grain and grain boundaries is very different. This difference may be the reason for the observed inhomogeneous charging.

When secondary electron emission surpasses the primary electron dose during higher energy electron irradiation, the sample builds up a positive charge. Each emitted secondary electron should increase the positive surface charge because of the low conductivity of the sample; however, the positive charge can be neutralized by electrons attracted back to the surface. This charge neutralization will ultimately limit the amount of positive charge the sample can accumulate. In contrast to positive charging, negative charging has a natural limit determined by the energy of the primary electron beam. The charging will stop only when the surface potential repels the primary electrons. Another possible reason for the different efficiency of positive and negative sample charging might be different types of radiation-induced conductivity – hole-type or electron-type. At low energies we inject excess electrons, but at high energies we produce holes. If their mobilities are very different and they are the main free charge carriers, then efficiency of discharging could be very different.

## 4. Conclusion

The use of externally applied potentials to dielectric metal oxides was demonstrated to be a simple way of investigating the electron beam-induced charging during the process of electron-stimulated ion emission. The influence of surface potential on ion yield and kinetic energy was experimentally established and applied to the study of electron-induced charging of GDC. Externally applied positive potentials increase the cation kinetic energies linearly and negative potentials reduce the cation yields exponentially. The GDC surface can be charged either positively or negatively by electron beam bombardment, depending on the energy of the primary electrons. Irradiation by high-energy electrons (e.g., 400 eV electrons) produces a positive surface potential while irradiation by low-energy electrons (e.g., 75 eV electrons) generates a negative sample potential. Electron beam-induced positive charge by high-energy electron irradiation can be neutralized by subsequent low-energy electron irradiation and vice versa. These observations suggest efficient trapping of both the holes and the electrons by GDC surface. The grain boundary, with the presence of excess gadolinium ions $Gd^{3+}$ and oxygen vacancies, can provide the hole traps as well as electron traps, respectively.

## Acknowledgement

This work was supported by the United States Department of Energy USDoE-NETL SECA Core Technology Program under Grant No. DE-FC26-02NT41572 and USDoE Nuclear Energy Research Initiative (NERI) under Grant No. DE-FG03-00SF22207.

## References

[1] N.Q. Minh, J. Am. Ceram. Soc. 76 (1993) 563.
[2] S. De Souza, S.J. Visco, L.C. De Jonghe, J. Electrochem. Soc. 144 (1997) 35.
[3] T. Suzuki, I. Kosacki, H.U. Anderson, Solid State Ionics 151 (2002) 111.
[4] S.C. Singhal, Solid State Ionics 152–153 (2002) 405.
[5] C. Xia, M. Liu, Adv. Mater. 14 (2002) 521.
[6] R.M. Ormerod, Chem. Soc. Rev. 32 (2003) 17.
[7] H. Inaba, H. Tagawa, Solid State Ionics 83 (1996) 1.
[8] B.C.H. Steele, Solid State Ionics 129 (2000) 95.
[9] C. Xia, M. Liu, Solid State Ionics 152–153 (2002) 423.
[10] P.S. Manning, J.D. Sirman, J.A. Kilner, Solid State Ionics 93 (1996) 125.
[11] E. Ruiz-Trejo, J.D. Sirman, Y.M. Baikov, J.A. Kilner, Solid State Ionics 113–115 (1998) 565.
[12] J.A. Lane, J.A. Kilner, Solid State Ionics 136–137 (2000) 927.
[13] R.D. Ramsier, J.T. Yates Jr., Surf. Sci. Rep. 12 (1991) 243.
[14] J.L. de Segovia, E.M. Williams, Chem. Phys. Solid Surf. 9 (2001) 608.

[15] T. Gotoh, S. Takagi, G. Tominaga, Vacuum 41 (1990) 213.
[16] I. Colera, E. Soria, J.L. De Segovia, E.L. Roman, R. Gonzalez, Vacuum 48 (1997) 647.
[17] M.C. Torquemada, J.L. de Segovia, E. Roman, Surf. Sci. 337 (1995) 31.
[18] W.C. Simpson, W.K. Wang, J.A. Yarmoff, T.M. Orlando, Surf. Sci. 423 (1999) 225.
[19] T.M. Orlando, A.B. Aleksandrov, J. Herring, J. Phys. Chem. B 107 (2003) 9370.
[20] Y. Lei, Y. Ito, N.D. Browning, T.J. Mazanec, J. Am. Ceram. Soc. 85 (2002) 2359.
[21] H. Norenberg, G.A.D. Briggs, Phys. Rev. Lett. 79 (1997) 4222.
[22] M.L. Knotek, P.J. Feibelman, Phys. Rev. Lett. 40 (1978) 964.
[23] H. Chen, A. Aleksandrov, Y. Chen, J. Dong, M. Liu, T.M. Orlando, in preparation.
[24] J. Herring, A. Aleksandrov, T.M. Orlando, Phys. Rev. Lett. 92 (2004) 187602.
[25] V.V. Afanas'ev, A. Stesmans, Appl. Phys. Lett. 80 (2002) 1261.
[26] V.V. Afanas'ev, A. Stesmans, J. Appl. Phys. 95 (2004) 2518.
[27] A.B. Aleksandrov, E.D. Aluker, I.A. Vasiliev, A.F. Nechaev, Introduction Radiat. Phys. Chem. Alkali Halide Cryst. Interf. 8 (1989) 200.
[28] W.C. Simpson, T.M. Orlando, L. Parenteau, K. Nagesha, L. Sanche, J. Chem. Phys. 108 (1998) 5027.
[29] A.D. Bass, P. Cloutier, L. Sanche, J. Appl. Phys. 84 (1998) 2740.
[30] B. Vallayer, G. Blaise, D. Treheux, Rev. Sci. Instrum. 70 (1999) 3102.
[31] J. Liebault, K. Zarbout, D. Moya-Siesse, J. Bernardini, G. Moya, Appl. Surf. Sci. 212–213 (2003) 809.
[32] H. Inaba, R. Sagawa, H. Hayashi, K. Kawamura, Solid State Ionics 122 (1999) 95.